Simulation Modelling Practice and Theory 53 (2015) 1–14

Contents lists available at ScienceDirect

Simulation Modelling Practice and Theory

journal homepage: www.elsevier.com/locate/simpat

# On the introduction of adaptive mass scaling in a finite element model of Ti6Al4V orthogonal cutting

F. Ducobu *, E. Rivière-Lorphèvre, E. Filippi

*University of Mons (UMONS), Faculty of Engineering (FPMs), Machine Design and Production Engineering Department, 20 Place du Parc, B-7000 Mons, Belgium*

ARTICLE INFO

*Article history:*
Received 27 August 2014
Received in revised form 30 December 2014
Accepted 5 February 2015

*Keywords:*
Finite element modelling
Mass scaling
Orthogonal cutting
Titanium alloy Ti6Al4V

ABSTRACT

Machining by chips removal operations depend on a large set of parameters, which leads to a time consuming and expensive experimental optimization of this process. Numerical finite element modelling of orthogonal cutting is its most attractive alternative at this time. Apart from the difficulties caused by the complexity of the phenomena involved, the industrial application of this method comes up against unacceptable CPU computing time. The mass scaling is a numerical technique allowing to artificially speed up these calculations. This paper presents its application to a Lagrangian orthogonal cutting finite element model of the most commonly machined titanium alloy, Ti6Al4V, which has not previously been performed. Once the adaptive mass scaling is enabled, the CPU computing time is reduced by about 70% for a typical computation. This improvement should not be performed at the expense of the quality of the results by comparison to the experimental reference (chip morphology, formation mechanism, cutting forces, teeth formation frequency, etc.), nor impact significantly the numerical computation (total mass increase of the model, for example). This study shows that, when used carefully, the adaptive mass scaling constitutes an efficient method to reduce the CPU computation time. It should therefore be considered for the development of future models.



## 1. Introduction

Machining by removing of chips is a technique used for many years but due to the large set of parameters (cutting conditions, tool, material, etc.) that it involves, its optimization is far from being achieved and there is still much work to do in this field [1]. This is even more crucial when the machined material is a hard-to-cut material such as a titanium alloy [2]. It especially implies that research of optimal conditions by trial and error is often difficult and time consuming. Various methods have been developed to make this a more objective and efficient task, as for example the design of experiment (DOE) [3] using Tagushi's method [4,3], split-plot DOE [3], group method of data handling (GMDH) [3], the Response Surface Methodology (RSM) [3] or the method of the tool-material couple [5–7]. Although they can significantly reduce the number of experiments to perform, they however still consume a lot of time and money [3] (whether manpower or the cost of the tools and the machined material).

Numerical modelling of orthogonal cutting can be used to address this problem [8,9]. Moreover, numerical models provide access to experimental hard-to-measure information such as temperatures at the tool – chip interface [9,10], shear stresses [9], plastic strain and plastic strain rate [9,11] or residual stresses in the machined workpiece [9,12], for example.

* Corresponding author. Tel.: +32 65 45 47; fax: +32 65 45 45.
*E-mail address:* Francois.Ducobu@umons.ac.be (F. Ducobu).

http://dx.doi.org/10.1016/j.simpat.2015.02.003
1569-190X/

However, it must be admitted that current models and computing resources are not yet ready for an industrial application, as highlighted by Filice et al. [13]. Two main difficulties have therefore still to be addressed [1,14]: the model development and the computation time. Indeed, developing a model that reproduces accurately experimental results and respects the physics of the phenomena is not easy (as well as its validation [1], especially because the most influencing parameter is friction while it cannot precisely be measured [9]) and getting results in a reasonable CPU computing time is still a challenge [1,3].

Although the computing power increased exponentially in a few decades [1,15] and robust calculation algorithms are available through finite element modelling programs [1], the complexity of the phenomena is such that the computing time is still too large. It is ordinary to have computing lasting for several days, indeed several weeks even for simplified geometries (case of two-dimensional orthogonal cutting) and a short simulated time (well below 1 mm cutting length). The industrial application of such numerical models must therefore pass through a reduction of the CPU computing time without sacrificing the quality of the results.

Different methods have been studied to artificially accelerate this type of numerical calculations. The increase at the beginning of the resolution of some material properties (specific heat [16], for example) or the modification of the cutting conditions (cutting speed [17], for example), i.e. the load factoring, are two first methods. They must of course ensure that the results are not influenced too much, which seems unlikely for the cutting speed.

More advanced numerical methods to artificially accelerate the calculations were developed such as the mass scaling [18–20], the parallel computing [21], the multi-grid methods [21] or more recently the Graphic Processing Unit (GPU) computing [22]. In this paper, mass scaling is introduced in a numerical model experimentally validated with a single CPU core [14] and its influence on the results is studied. This has not previously been performed for a Lagrangian finite element model of orthogonal cutting.

For this purpose, the main characteristics of the original finite element model are first presented. The concept of mass scaling is then defined and its introduction in the model is performed. Finally, numerical results with mass scaling are compared to previous numerical results (without mass scaling) and experimental tests in order to show the influence of this technique on the results and its interest.

## 2. Main characteristics of the model developed

A thermomechanical finite element model was developed using the commercial software Abaqus/Explicit v6.8. It consists of a two-dimensional orthogonal cutting model in plane strain condition. It only takes account of the area near the edge radius of the tool. The machined material is Ti6Al4V, a titanium alloy, and the tool material is tungsten carbide.

In order to compare the cutting forces and the geometry of the saw-toothed chip obtained by numerical simulation to those obtained experimentally, the model adopts, as much as possible, the same cutting conditions as the reference article of Sun et al. [23].

As the model concerns the transient phase of the chip formation, the Lagrangian formulation is chosen over the Eulerian and the Arbitrary Lagrangian Eulerian (ALE) ones [1,3]. In order to allow the chip separation from the workpiece, a damage criterion must be adopted because of the Lagrangian formulation [1]. The chosen criterion is based on the eroding elements method [24] and involves the use of the temperature dependent tensile failure of Ti6Al4V [14]. This chip separation criterion is a key parameter to obtain realistic simulations [25]. In this model, the suppression of a finite element introduces a crack in the workpiece, making it possible for the chip to come off.

### 2.1. Geometry and boundary conditions

The initial geometry and boundary conditions are presented in Fig. 1.

The workpiece to machine is modelled as a rectangular box measuring 1.5 mm long and 1 mm thick. The tool is modelled with a cutting edge radius of 20 μm, a rake angle of 15° and a clearance angle of 2°. The depth of cut, $h$, is 0.28 mm.

Concerning the boundary conditions, the workpiece is fixed while the cutting tool moves. The under edge and the left edge of the workpiece are constrained against horizontal and vertical displacements. The tool has its upper and right sides

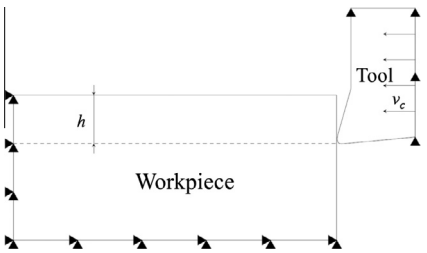


**Fig. 1.** Initial geometry and boundary conditions of the model.

constrained against vertical displacement. It moves towards the workpiece (and therefore to the left in Fig. 1) at the cutting speed, $V_c$, of 75 m/min.

### 2.2. Behaviour of the materials

The chip obtained experimentally in these cutting conditions is a saw-toothed one, as shown by Sun et al. [23] in their experiments. The model must therefore produce such a chip [14]. The behaviour of the Ti6Al4V (assumed as homogeneous and isotropic) is described by the Hyperbolic TANgent law (TANH), introduced by Calamaz et al. [26]. It consists in a modified version of the Johnson–Cook law [27] taking into account the strain softening of the material.

The Johnson–Cook law [27] is the most popular constitutive model adopted in cutting process simulation. It dissociates plastic, viscous and thermal aspects in three independent terms:

$$\sigma = (A + B\ \varepsilon^n)\left(1 + C\ \ln\frac{\dot{\varepsilon}}{\dot{\varepsilon}_0}\right)\left(1 - \left[\frac{T - T_{room}}{T_{melt} - T_{room}}\right]^m\right) \tag{1}$$

where $T_{melt}$ is the melting temperature, $T_{room}$ is the room temperature (298 K) and $\dot{\varepsilon}_0$ is the reference strain rate. $A, B, C, m$ and $n$ are material properties. Table 1 presents the set of parameters used for this study.

As the formation of a saw-toothed chip may be due to the strain softening of the material, Calamaz et al. [26] propose to upgrade the Johnson–Cook law to the Hyperbolic TANgent law by introducing this softening into the material behaviour law (Fig. 2). It is expressed by the following equation [26]:

$$\sigma = \left[A + B\ \varepsilon^n\left(\frac{1}{\exp(\varepsilon^a)}\right)\right]\left[1 + C\ \ln\frac{\dot{\varepsilon}}{\dot{\varepsilon}_0}\right]\left[1 - \left(\frac{T - T_{room}}{T_{melt} - T_{room}}\right)^m\right]\left[D + (1 - D)\tanh\left(\frac{1}{(\varepsilon + S)^c}\right)\right] \tag{2}$$

with

$$D = 1 - \left(\frac{T}{T_{melt}}\right)^d \quad \text{and} \quad S = \left(\frac{T}{T_{melt}}\right)^b$$

Parameters $A, B, C, m$ and $n$ have the same meaning as for the Johnson–Cook law, while $a, b, c$ and $d$ are the new constants introduced by the TANH law. The parameters value are given in Table 2.

The conversion of the plastic deformation energy to heat is carried out with an efficiency of 90% [28].

**Table 1**
Parameters of the Johnson–Cook law for Ti6Al4V, from [28–30] (amongst others).

| J–C law parameters | |
|---|---|
| $A$ (MPa) | 862 |
| $B$ (MPa) | 331 |
| $C$ | 0.012 |
| $m$ | 0.8 |
| $n$ | 0.34 |
| $T_{melt}$ (K) | 1878 |

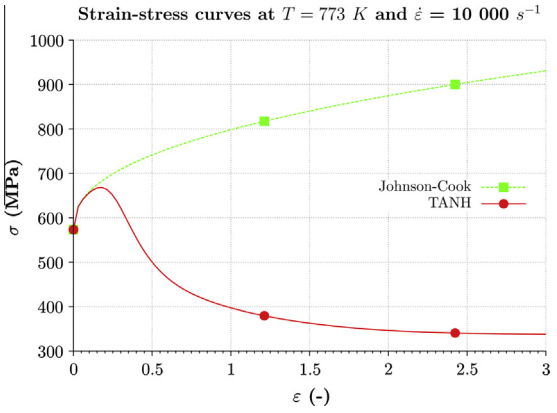


**Fig. 2.** Influence of the addition of the strain softening on the shape of the Johnson–Cook law.

**Table 2**
Parameters of the TANH law for Ti6Al4V, from [26].

| TANH law parameters | | | |
|---|---|---|---|
| $A$ (MPa) | 968 | $a$ | 1.6 |
| $B$ (MPa) | 380 | $b$ | 0.4 |
| $C$ | 0.02 | $c$ | 6 |
| $m$ | 0.577 | $d$ | 1 |
| $n$ | 0.421 | | |
| $T_{melt}$ (K) | 1878 | | |

**Table 3**
Materials properties, from [28–30,32].

| Material properties | Ti6Al4V | WC |
|---|---|---|
| Density (kg/m$^3$) | 4430 | 15,000 |
| Young's modulus (GPa) | 113.8 | 800 |
| Poisson's ratio (–) | 0.342 | 0.2 |
| Expansion (m/m K) | 8.6e$^{-6}$ | 4.7e$^{-6}$ |
| Thermal conductivity (W/m K) | 7.3 | 46 |
| Specific heat (J/kg/K) | 580 | 203 |

The behaviour of the tool material (tungsten carbide) is described by a linear elastic law. The material properties of Ti6Al4V and tungsten carbide are the same as the base model [14,31] and can be found in Table 3.

### 2.3. Friction and thermal aspects

The tool – workpiece contact is defined between the outer surface of the tool and all the nodes of the workpiece. Coulomb's friction (with a low coefficient value of 0.05 in accordance with Calamaz et al. [26] and Bäker et al. [33]) is adopted to model the interaction between the tool and the workpiece. All the energy it generates is converted into heat [34]. Only conduction is considered and all the boundaries are supposed to be adiabatic.

### 2.4. Mesh

Four-node linear (in displacement and temperature) elements compose the structured mesh of the upper part of the workpiece. The meshes of the tool and the lower part of the workpiece are composed of three- and four-node elements of the same type. The initial mesh is presented in Fig. 3, the workpiece is composed of roughly 22,000 elements and the tool of about 400.

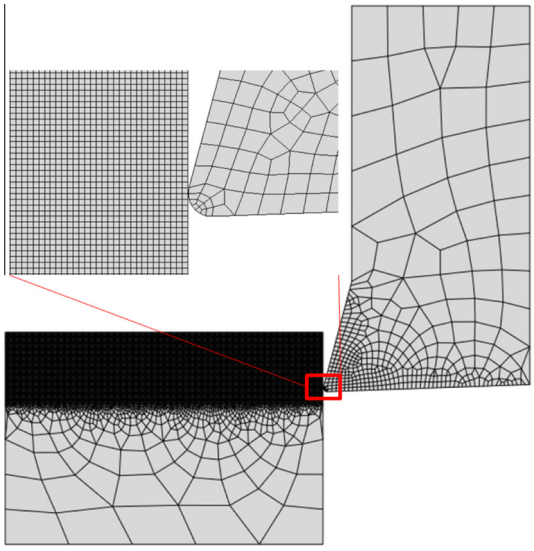

**Fig. 3.** Initial mesh of the model.

The number and the size of the elements composing the mesh result of a compromise between an acceptable CPU computing time and a sufficient accuracy. The size of the elements in the upper part of the workpiece where the chip is formed has been set to 5 μm to meet these requirements. Several criteria allowed convergence to this value.

First of all, the size of these elements must be less than the cutting edge radius of the tool, which is equal to 20 μm. This constraint is a necessary condition to take it into account.

Then, a good practice rule in finite element simulation is that an arc of a circle of 90° must be composed of at least four elements. As the cutting edge radius of the tool is 20 μm, the length of such an arc is 31.42 μm. The size of the elements should then be maximum 7.86 μm.

The chosen value of 5 μm meets well both conditions. To reduce the number of elements, and therefore the CPU computing time, the lower part of the workpiece uses a coarser mesh, as shown in Fig. 3. This reduction can be achieved without adversely affecting the quality of the model since the concerned elements are away from the cutting area.

## 3. Introduction of the mass scaling

### 3.1. The explicit method

The direct integration scheme adopted for the resolution is explicit. It is chosen over the implicit integration scheme as it is well suited to solve problems dominated by numerous nonlinearities such as these encountered in the model developed: dynamic phenomena, nonlinear materials behaviour, introduction of thermal effects, contact,... Indeed, although many integration steps are necessary in the explicit resolution, it is often much faster than the implicit one. The absence of iterations and tangent stiffness matrix are the main reasons [35]. The contact management and thermal coupling are taken into account more easily and quickly in explicit [35]. An other advantage of explicit over implicit resolution is that the size of the increment only depends on the element dimensions and material properties and not on the complexity of the analysis [19].

The explicit scheme allows, from the solution at the current time step, to calculate the solution at the next time step. For this purpose, the total time of the analysis ($D$) is divided into a large number ($n$) of time intervals $\Delta t$ (and $\Delta t = \frac{D}{n}$). An approximation of the solution is then determined at times $0, \Delta t, 2\Delta t, \ldots, t, t+\Delta t, \ldots, D$ [36]. In Abaqus/Explicit, the integration of the equations is done via the central difference method [37] and the speed is calculated assuming that the acceleration is constant over this short period of time [35,36,38]:

$$U_{t+\Delta t} = U_t + \Delta t_{t+\Delta t}\, \dot{U}_{t+\frac{\Delta t}{2}} \tag{3}$$

$$\dot{U}_{t+\frac{\Delta t}{2}} = \dot{U}_{t-\frac{\Delta t}{2}} + \frac{1}{2}(\Delta t_{t+\Delta t} + \Delta t_t)\, \ddot{U}_t \tag{4}$$

with $U$ the displacement vector, $\dot{U}$ the speed vector and $\ddot{U}$ the acceleration vector.

Acceleration is given by

$$\ddot{U}_t = M^{-1} \cdot (F_t - I_t) \tag{5}$$

where $M$ is the (diagonal) mass matrix, $F$ is the vector of applied forces and $I$ is the vector of internal forces.

Since the solution depends on the solution at the previous step, this type of scheme requires a special procedure to start:

$$\dot{U}_{-\frac{\Delta t}{2}} = \dot{U}_0 - \frac{\Delta t_0}{2}\ddot{U}_0 \tag{6}$$

#### 3.1.1. Numerical stability

Explicit integration methods are called conditionally stable because they require that the time increment value is less than a critical value $\Delta t_{crit}$. The choice of the time increment value is not a simple problem. It results of a compromise between stability and accuracy. Indeed, it should be small enough so that the solution is accurate, but not too much to prevent a CPU cost higher than necessary, as the number of operations is directly proportional to the number of time steps required to obtain the solution [36].

Since the problem is thermally coupled, the critical time increment should be calculated for the mechanical and thermal (involving the Fourier number [39]) aspects [37]. In practice, the stability is determined by the mechanics, the thermal time increment being much higher than the mechanical one (with a ratio of more than 10,000 for this model).

The critical time increment is calculated from the properties of mass and stiffness of the entire system. Without damping it is given by Ref. [19,20,35,36,38]

$$\Delta t \leqslant \Delta t_{crit} = \frac{T_{min}}{\pi} = \frac{2}{\omega_{max}} \tag{7}$$

where $T_{min}$ is the smallest eigenvalue of the finite element model and $\omega_{max}$ is the largest eigenfrequency.

In practice, to avoid having to calculate the eigenvalues [35], the stability limit is calculated by

$$\Delta t_{crit} = min\left(\frac{L_c}{C_d}\right) \tag{8}$$

with $L_c$ the characteristic length of each element of the mesh and $C_d$ the wave propagation speed in the material. This time increment corresponds to the time required for a compressive wave to pass through the smallest element of the model. To give an order of magnitude for Ti6Al4V and with a minimum element length of 5 μm, the time increment without damping is equal to $9.56e^{-10}$ s.

The expression of the critical time increment written in this form corresponds to the condition on the CFL (Courant–Friedrichs–Lewy) number [20]:

$$\text{CFL} = \frac{C_d \cdot \Delta t}{L_{min}} \leqslant 1 \tag{9}$$

A single element of the mesh can therefore lead to a major increase in CPU computing time. In this model, when the tool moves, the elements located near the tool edge radius are strongly deformed and the value of their time increment decreases significantly. Once the cutting process has started, the global time increment is then greatly reduced because of these few elements. This results in a significant lengthening of the CPU computation.

### 3.2. Computing time reduction

We have seen in Section 3.1 that the total number of increments is equal to $n = \frac{D}{\Delta t}$ and in Section 2.4 that the mesh cannot be further modified. Two main alternatives coexist therefore to reduce the CPU computing time [19]: reduce the total time $D$ or increase the time increment $\Delta t$. The first method is called "load factoring" while the second is the "mass scaling".

#### 3.2.1. Load factoring

The goal of the load factoring is to reduce the total time of the analysis. It is achieved by applying boundary conditions and loads over a shorter period of time [19]. In order to obtain accurate results, the material properties cannot be rate dependent and the influence of the inertia effects must be limited. Prior [19] therefore recommends to limit the kinetic energy to less than 5% of the strain energy.

In machining it could easily be achieved by considering a larger cutting speed. However, it is well-known that the cutting speed affects the mechanism of chip formation and is one of the critical parameters of this process. Moreover Ti6Al4V exhibits strain rate dependence. This method can therefore not be used to speed up the computing time in orthogonal cutting of Ti6Al4V without significantly affecting the process.

#### 3.2.2. Mass scaling

The mass scaling (MS) is the artificial increase of the mass of an element of the mesh to increase the value of the time increment. It can be performed trough the increase of the material density [18–20]. Prior [19] and Wang and Guo [38] present applications of mass scaling in metal forming (deep drawing and hot ring rolling). A noticeable advantage of the method is that this change in the material density does not affect the rate dependence of the material.

Mass scaling can be implemented through different ways. The more "basic" one is the full mass scaling in which the mass of every element is scaled [37]. In our model, only some deformed element near the tool edge radius and in the chip need to be scaled. Moreover, increasing the mass of large elements (those composing the right part the tool for example) would influence the results of the model due to the increase of the inertia effects.

Adaptive mass scaling is adopted in this paper. This method increases the mass of the elements whose time incrementation value is less than a limit value set before the launch of the calculation [37]. The global time incrementation of the model is equal to this limit value when the elements near the tool edge radius are very deformed. Mass scaling thus allows to counter the decrease of the overall time incrementation by raising the local times incrementation lower than a given limit. The quantity by which the time increment of the element for which the mass scaling is active is multiplied is called the "mass scaling factor". In this application, this factor will be different for each element of the mesh and will vary at each time increment.

Mass scaling artificially increases the mass of elements. It is therefore essential to remain aware that adding some "non-physical" mass to increase the time increment can strongly affect the results, especially for a dynamic study and the inertia effects could become dominant. A common technique to check a posteriori that the mass scaling does not significantly affect the results is the comparison between the kinetic energy and the internal energy of the system. This ratio is often chosen below 5–10% [38,40,41]. Zybell [40] also recommends ensuring that the work applied by external forces remains close to the internal energy.

## 4. Determination of the minimum time increment value

In order to determine the acceptable level of mass scaling, it is necessary to run several analyses with different values of the minimum time increment allowed. Six values of the minimum time increment are considered in this paper. At the beginning of an analysis without mass scaling, the time increment value adopted by Abaqus/Explicit is equal to $51.1e^{-11}$ s. The first

time increment considered in this study is approximately equal to this initial value: $50e^{-11}$ s. Then smaller values are chosen: 2% ($1e^{-11}$ s), 5% ($2.5e^{-11}$ s), 10% ($5e^{-11}$ s), 20% ($10e^{-11}$ s) and 50% ($25e^{-11}$ s) of the first one.

Assuming that a numerical chip morphology close to the experimental one is a necessary condition to validate the model, only this aspect will be kept to conclude on the maximal value that can be adopted for the minimum time increment. To compare relevant results, a moment in the chip formation is chosen: the beginning of the third tooth formation, at the time where stresses begin to fall in the primary shear zone.

Chips morphologies obtained for the time increment values considered are presented in Fig. 4 and compared to the experiments (Fig. 4(a)). Morphologies from (b) to (e), as well as the Von Mises stresses contours, are close to each other and to the experimental one (a). It is noted that a crack appears in the second tooth for chips (d) and (e), contrary to the others. An important change occurs for the last three morphologies (from (f) to (h)) as the chip becomes discontinuous. Mass scaling influences the morphology too much and the three corresponding time increment values are therefore too large. The maximum time increment value that can be used, based on chip morphology, is $5e^{-11}$ s.

Table 4 shows the CPU computing time with a single 3 GHz Intel processor for each model. For the comparison to be relevant, the CPU computing time is given at the same simulation length for all the models. Without mass scaling, the third tooth of the chip begins to form after 320 μs; this value will be used.

The action of mass scaling is clearly noticed and the computing time is reduced when the time increment value increases. Even the lowest value of the time increment ($1e^{-11}$ s) leads to a significant CPU computing time reduction. It also shows that the percent change in mass for the whole model increases with the time increment value, as expected. For the $5e^{-11}$ s time increment, it is negligible ($1.89e^{-2}$%), contrary to the highest value considered in this study (6.38%). This confirms that this value can be used for the rest of the study. Table 4 also shows that at 320 μs of simulation time the mass increase of the model for the two lowest time increment values ($1e^{-11}$ s and $2.5e^{-11}$ s) is too small to be measured.

## 5. Influence of the mass scaling on the results

Now that the maximal time increment value for mass scaling is determined ($5e^{-11}$ s), a more detailed comparison with the case without mass scaling will be performed.

### 5.1. Morphology and chip formation

Concerning the chip morphology and its formation, the comparison reveals, as stated before, that the two numerical chips are very similar. Few differences are identified. The first one is the simulation length: the third tooth of the chip begins to

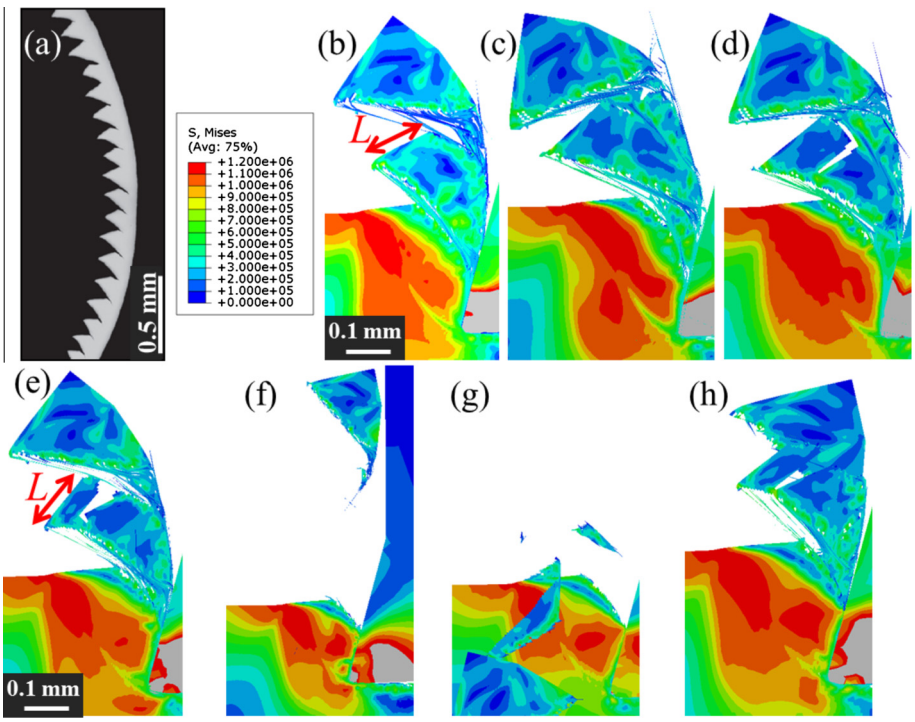


**Fig. 4.** Comparison of the chips (a) obtained experimentally [23] and modelled (b) without mass scaling, with mass scaling (c) $\Delta t = 1e^{-11}$ s, (d) $\Delta t = 2.5e^{-11}$ s, (e) $\Delta t = 5e^{-11}$ s, (f) $\Delta t = 10e^{-11}$ s, (g) $\Delta t = 25e^{-11}$ s and (h) $\Delta t = 50e^{-11}$ s (Von Mises stresses, $e^3$ Pa) at the beginning of the third tooth formation.

**Table 4**
Mass scaling (MS) influence at 320 μs of simulation time.

| $\Delta t$ | Computing time (h) | Mass increase (%) |
|---|---|---|
| Without MS | 93h34 | – |
| $1e^{-11}$ s | 76h04 | 0 |
| $2.5e^{-11}$ s | 40h40 | 0 |
| $5e^{-11}$ s | 25h27 | $1.89e^{-2}$ |
| $10e^{-11}$ s | 13h30 | $4.59e^{-2}$ |
| $25e^{-11}$ s | 6h10 | $1.70e^{-1}$ |
| $50e^{-11}$ s | 4h43 | 6.38 |

form after 320 μs in the case without mass scaling (Fig. 4(b)) while 340 μs are needed in the second case (Fig. 4(e)). This discrepancy remains very low (approximately 6%). It explains, however, why the tooth of the case with mass scaling is slightly more pronounced and why the chip is a bit more curved as the simulation length is larger in this case. Another difference is the presence of a crack in the second tooth when mass scaling is activated. Except on the morphology of the second tooth, this crack has no influence on the results (cutting forces, contact length and teeth formation frequency).

In comparison with the experimental reference chip [23], it turns out that the two numerical chips are very close to each others. Table 5 shows the comparison of the undeformed tooth length, $L$, value for the three chips. It corresponds to the length shown in Fig. 4. For numerical chips, this is the length of the second tooth (the first tooth is not considered because it is formed when the tool enters into the material), while for the experimental chip, this is the average length measured on approximately 50 teeth.

The three lengths are very close to each other and the difference with the reference [23] rises respectively without and with mass scaling to 15% and 16%. The difference between the lengths given by the two models is smaller than 2%, which is very low. It confirms that the morphology of three chips is similar and that mass scaling does not influence it significantly.

Another important feature that the model must maintain is the saw-toothed chip formation mechanism. It turns out that for both models the formation occurs in two times, as expected [14], and involves the adiabatic shear band and the crack propagation. The mass scaling introduction in the model therefore does not alter the phenomena involved in the saw-toothed Ti6Al4V chip formation in orthogonal cutting.

### 5.2. Computing time

The aim of the mass scaling introduction is the CPU computing time reduction. In Section 4, Table 4 showed the magnitude of this reduction after 320 μs of simulation. Let have a closer look at the necessary time to reach the beginning of the third tooth formation. In the case without mass scaling, 93 h 34 min of CPU time are needed to calculate 320 μs of simulation. When mass scaling is enabled, only 37 h 21 min of CPU time are required to calculate 340 μs of simulation. Mass scaling provides thus an economy of about 65 h CPU computing time, corresponding to a gain of almost 71%.

Mass scaling produces therefore the expected result after it comes into action. It is now imperative to ensure that this gain in computation time is not done to the detriment of the quality of the results. It has already been highlighted that its influence on the chip morphology is minimal and it is moreover negligible on the chip formation mechanism.

### 5.3. Contact length

An important value in the comparison of the two chips formation is the contact length between the chip and the tool on the rake face. To do this, it seems unwise to compare different simulation times: a longer time implies a longer distance travelled by the tool, which has an influence on the contact length. It was therefore chosen to compare these lengths at the same moments. After 320 μs of simulation, the contact length is the same in both cases and is approximately equal to 218 μm. After 340 μs of simulation time, it is still the same for both cases and amounts to approximately 238 μm. It is therefore proved that mass scaling does not affect the contact length between the chip and the tool.

### 5.4. Numerical influence on the results

As announced in paragraph Section 3.2.2, the action of the mass scaling is reflected by the increase of the mass of some elements and the factor multiplying the time increment value is called the mass scaling factor. To give an idea of its order of

**Table 5**
Undeformed tooth length values.

| | Reference | Without MS | With MS |
|---|---|---|---|
| $L$ (μm) | 130 | 152 | 155 |

magnitude, at 340 μs of simulation time, the maximum mass scaling factor for the model is 3.21, a rather low value. This means that the extent of the mass scaling is quite limited.

In addition, as shown in Fig. 5, the mass of very few elements is artificially increased. In general, the relevant elements are located on the edges of the teeth and on the machined surface. It is in addition noted that the majority of these elements is affected by a mass scaling factor inferior to 1.5 at 340 μs of simulation time.

The increase of the total mass of the model due to the mass scaling is equal to approximately $2e^{-2}$% after 340 μs of simulation. It therefore remains very small and can be considered as negligible (which has already been shown by the mass increase of the whole model in Table 4 after 320 μs of simulation).

As presented in paragraph Section 3.2.2, the literature recommends that the kinetic energy stays below 5–10% of the internal energy when the mass scaling is activated. Fig. 6 presents the evolution (in %) of the ratio between the internal energy and the kinetic energy versus time. Except a peak at about 16% after 5 μs (and thus far before the activation of mass scaling), the ratio is well below 1%. This criterion is therefore fulfilled. It is also recommended for the work applied by the external forces to stay close to the internal energy. In Fig. 6, it is noted that the two energies are very close to each other. The difference between them grows in time to reach nearly 5% after 320 μs, which is low and shows that this criterion is also satisfied.

As a conclusion, it turns out that, except the CPU computing time reduction, the mass scaling has therefore virtually no significant numerical influence on the model results. The small number of elements affected by the mass scaling at 340 μs (Fig. 5) confirms that the significant increase in the CPU computing time in the absence of mass scaling is due to the negative influence of a small smattering of elements on the time incrementation.

### 5.5. Cutting forces

Similarly to the morphology, the forces evolution and level are very close to each other, as shown in Fig. 7.

The cutting force evolution is cyclic, which is expected of a saw-toothed chip formation. Indeed, a drop in the force evolution is observed during the formation of a tooth. The experimental reference force of Sun et al. [23] is constant: this is the root mean square (RMS) value of the measured signal.

It is noted that, at the beginning of the operation, the forces with and without mass scaling are identical, which is not surprising since the mass scaling is not yet entered into action. A small difference appears then. It is important to keep in mind that the phenomena involved are highly numerically unstable due to nonlinearities. Therefore, a weak disturbance can lead to very different results. In this case, the disturbance is the mass scaling. It is consequently quite normal to get such results.

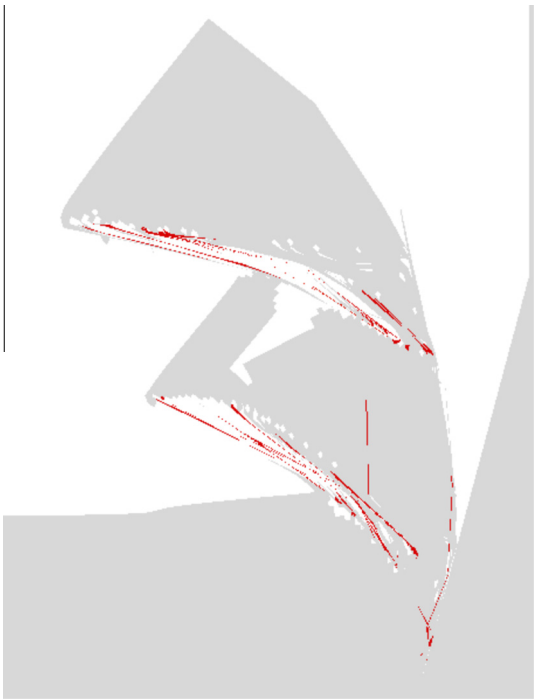

**Fig. 5.** Elements affected by the mass scaling at 340 μs of simulation time.

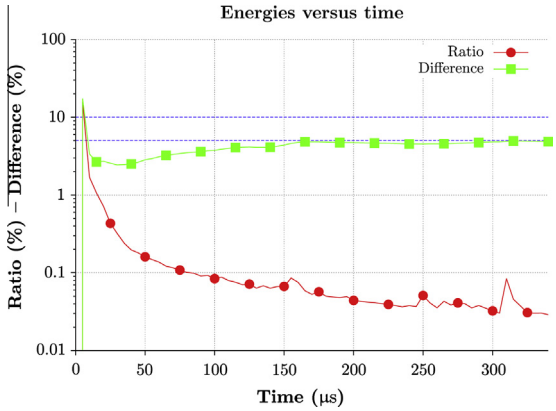


**Fig. 6.** Evolution of the ratio of the kinetic and internal energies ("Ratio") and the difference between the work applied by the external forces and the internal energy ("Difference").

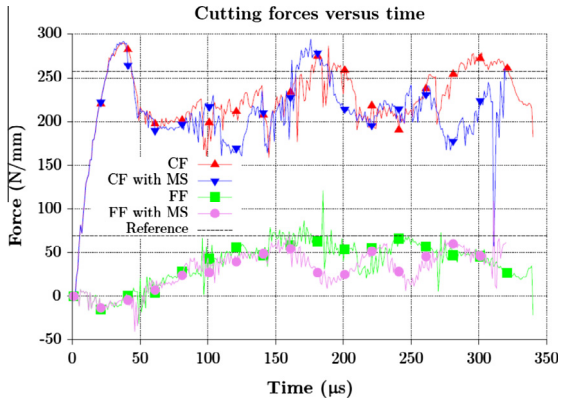


**Fig. 7.** Comparison of the cutting (CF) and feed forces (FF) with and without mass scaling with the reference of Sun et al. [23].

A shift of the order of 20 µs between the cutting forces is identified. A more significant difference is observed regarding the feed forces. In addition, without mass scaling, the feed force evolution is hardly linkable with the cutting force. The activation of the mass scaling seems to reduce this inconvenience. Indeed, except for the first tooth corresponding to the entrance of the tool in the workpiece, there is a small offset between the maxima of the cutting force and the minima of the feed force, which seems to be in advance.

Regarding the comparison between numerical and experimental values, Fig. 7 shows that the results are very close in all three cases, especially for the cutting one. Table 6 quantifies this comparison based on the RMS values.

It is noted that, as shown in Fig. 7, differences are smaller for the cutting force than for the feed force. The reference cutting force of Sun et al. [23] is 12% and 16% larger than the modelling, respectively, without and with mass scaling. The difference between the two numerical models is 4%. For the feed force, these values are 33%, 45% and 17%.

Small variations on the forces signals (that can be seen as a kind of noise) are observed. They are mostly due to the elements suppression: each element deletion has the same result on the forces as a small impact, perturbing the stability of the numerical modelling. These high frequency variations of small magnitude could affect the chip formation (and its morphology) and the stability of the process. No significant difference is observed (Fig. 7) on that aspect when mass scaling is enabled.

When the cutting length is longer than a few millimetres, tool wear is another source of cutting forces alteration: forces increase are observed and the feed force is usually more affected than the cutting force [42]. The tool wear plays a significant

**Table 6**
RMS values of the forces.

| | Reference | Without MS | With MS |
|---|---|---|---|
| CF (N/mm) | 257 | 227 | 217 |
| FF (N/mm) | 69 | 46 | 38 |

role in the machining costs especially as it depends on the cutting speed and the feed rate for a given material [43]. Tool wear monitoring is therefore a major area of research [43,44]. The numerical prediction of the tool wear is a difficult topic because of the multiple mechanisms and parameters it involves. Finite element models taking into account the tool wear can be found in the literature [45], some of them with an updating tool geometry depending on the wear evolution [46–50]. In this paper, the numerical simulation is run for a maximum of 1000 μs (see Section 5.6.3), i.e. 1.25 mm. As highlighted by Yen et al. [46], this is too short to perform a tool wear prediction. Future developments of the presented model will be focused on that point.

### 5.6. Teeth formation frequency

A last interesting feature to take into account in the comparison is the teeth formation frequency. Three different method are used in this paper to estimate it: based on the chip geometry, from the cutting force evolution and by fitting the best sine in a least squares way on the cutting forces signal.

#### 5.6.1. Chip geometry

The formation frequency can be estimated from $L$, the undeformed tooth length. This frequency, $F_g$, is given by Ref. [23]:

$$F_g = \frac{V_c}{L} \tag{10}$$

As for the chip geometry (see Section 5.1), the first tooth is not considered. The third one is not either since it is not completely formed. This estimation is therefore only based on the formation of the second tooth.

The frequency obtained with this method is very close in all three cases: 9615 Hz for the reference, 8224 Hz and 8065 Hz without and with mass scaling. Due to the method of calculation, the differences are identical to those calculated for $L$ (see Section 5.1).

#### 5.6.2. Cutting force evolution

In the case without mass scaling, it has been estimated from the cutting force evolution in Fig. 7 that the second tooth is formed in approximately 132 μs. With mass scaling, approximately 149 μs are required for the formation of the tooth. It ends to the following formation frequencies: $F_e = 1/(132e^{-6}) = 7576$ Hz for the first case and $F_e = 1/(149e^{-6}) = 6711$ Hz for the second.

As shown in Table 7, these values are of the same order of magnitude as the reference [23], although lower. The difference rises respectively without and with mass scaling to 21% and 30%. The difference between the frequencies given by the two models is 11%, which is low.

**Table 7**
Teeth formation frequencies according to the cutting force evolution ($F_e$).

| | Reference | Without MS | With MS |
|---|---|---|---|
| $F_e$ (Hz) | 9615 | 7576 | 6711 |

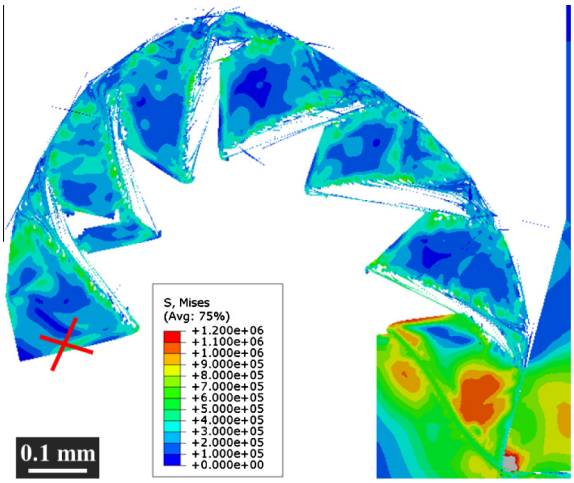


**Fig. 8.** Chip formed with mass scaling after 1000 μs of simulation time.

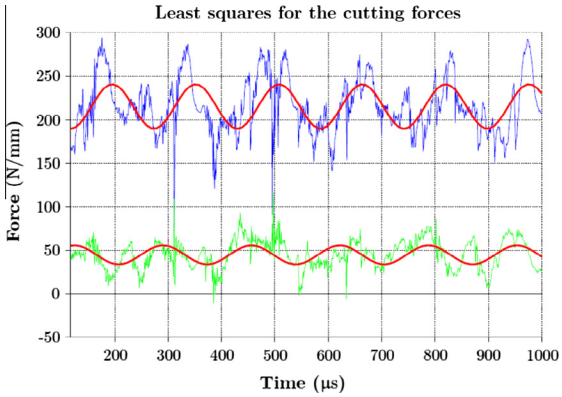


**Fig. 9.** Best sine in a least squares way for the cutting and feed forces.

*5.6.3. Least squares*

The forces evolution could be seen as a sine of frequency equal to that of the teeth formation of the chip and whose continuous component corresponds to the average effort. Following this observation, this paragraph proposes to adjust the best sine in a least squares way on the cutting forces signal.

Chips presented up to this point have only one single workable tooth, the second formed. It would result in an adjustment of the sine carried out on a single period, which is not judicious.

As previously presented (see Section 5.2), the CPU computing time without mass scaling is such that it is not reasonable to further continue the simulation. The case without mass scaling will therefore not be considered for the least squares method.

On the contrary, the gain in CPU computing time provided by the activation of the mass scaling allows a larger period of simulation; 1000 µs of simulation (leading to a bit more than 89 h of CPU computing time, which is still less than for 320 µs without mass scaling!) have been considered. The chip obtained presents 6 exploitable teeth (the first still being excluded) and it is shown in Fig. 8. In these conditions, it becomes possible to fit a sine on the force signal.

Fig. 9 shows this sine adjusted for the cutting and feed forces. The first sine presents a continuous component (zero offset), DC, of 215 N/mm, an amplitude of 26 N/mm and a frequency of 6402 Hz. The continuous component of the second is equal to 45 N/mm, its amplitude is 11 N/mm and its frequency is 6031 Hz. Tables 8 and 9 summarize these values.

The continuous components of the forces are very close to the RMS values presented in paragraph Section 5.5, Table 6. The difference for the tooth formation frequency based on the cutting force is 33% and 37% for the feed force. The difference between the frequencies given by the forces of the numerical model is 6%, which is very low. The observation of the forces evolution suggested the existence of such a difference between them.

*5.6.4. Conclusions of the teeth formation frequency*

The three methods lead to teeth formation frequencies of the same order of magnitude as the experimental reference of Sun et al. [23]. These simulated frequencies are all lower than the reference. The geometric method (paragraph Section 5.6.1), simple to apply on simulations results, led to the nearest value. Estimations based on the cutting force exhibit a larger

**Table 8**
Continuous components (DC) and frequencies via the least squares method for the cutting force.

| | Reference | CF |
|---|---|---|
| DC (N/mm) | 257 | 215 |
| $F_{CF}$ (Hz) | 9615 | 6402 |

**Table 9**
Continuous components (DC) and frequencies via the least squares method for the feed force.

| | Reference | FF |
|---|---|---|
| DC (N/mm) | 69 | 45 |
| $F_{FF}$ (Hz) | 9615 | 6031 |

difference with the experimental values. Finally, the method involving the least squares led to different frequencies depending on the force considered which could be guessed given their evolution.

In summary, the difference between the frequencies obtained by simulation and experimentally ranges from 16% to 37% depending on the selected method. The teeth formation frequency of the model is therefore close to the experimental value of Sun et al. [23]. The introduction of the mass scaling in the model leads to a difference from 2% to 11% depending on the method, the frequency obtained without mass scaling being always closer to the reference [23]. Mass scaling makes therefore the results deviate slightly further from the reference paper of Sun et al. [23] as compared to the results without mass scaling. The difference it introduces is, however, very small and it is negligible compared to the CPU computing time reduction it generates.

## 6. Conclusions

The mass scaling introduced to reduce the CPU computing time fulfils well its role: the gain is very important, of the order of 70%.

Moreover, the extent of its impact on the model is reduced. First of all from a strictly numerical point of view on the results. Indeed, few elements are concerned and the increase in the total mass of the model is negligible.

Then, the chip formation and the results are little influenced by mass scaling. The chips morphologies, the formation mechanisms, lengths of contact, forces and the teeth formation frequencies are very close with and without mass scaling. They are also all close to those of the experimental reference [23].

A model with adaptive mass scaling allows thus to obtain results very similar to a model without it but for a much more reasonable CPU computing time. It can (and should) therefore be considered for the development of future models.

## References


[1] in J. Davim (Ed.), Machining: Fundamentals and Recent Advances, Springer, 2008.
[2] J.P. Davim (Ed.), Machining of Titanium Alloys, Springer, 2014.
[3] in J.P. Davim (Ed.), Statistical and Computational Techniques in Manufacturing, Springer, 2012.
[4] R. Sabre, Plans d'expériences – Méthode de Tagushi, Techniques de l'Ingénieur F 1 006 (2007).
[5] NF E66-520-1 to 4, Working zones of cutting tools – couple tool-material for turning, 1997.
[6] NF E66-520-5 and 6, Working zones of cutting tools – couple tool-material for milling, 1999.
[7] NF E66-520-7 and 8, Working zones of cutting tools – couple tool-material for drilling, 2000.
[8] in J.P. Davim (Ed.), FEM in Manufacturing Processes, ISTE-Wiley, 2011.
[9] C. Maranhão, J.P. Davim, Finite element modelling of machining of AISI 316 steel: numerical simulation and experimental validation, Simul. Modell. Pract. Theory 18 (2010) 139–156.
[10] M. Jackson, M. Whitfield, J. Morrell, J.P. Davim, Computational analysis of the intimate contact between an inclined wedge and low carbon steel during metal cutting, Int. J. Mater. Prod. Technol. 37 (2010) 2–29.
[11] J.P. Davim, C. Maranhão, A study of plastic strain and plastic strain rate in machining of steel AISI 1045 using FEM analysis, Mater. Des. 30 (2009) 160–165.
[12] P. Arrazola, A. Kortabarria, A. Madariaga, J. Esnaola, E. Fernandez, C. Cappellini, D. Ulutan, T. Özel, On the machining induced residual stresses in IN718 nickel-based alloy: experiments and predictions with finite element simulation, Simul. Modell. Pract. Theory 41 (2014) 87–103.
[13] L. Filice, F. Micari, S. Rizzuti, D. Umbrello, Dependence of machining simulation effectiveness on material and friction modelling, Mach. Sci. Technol.: Int. J. 12 (2008) 370–389.
[14] F. Ducobu, E. Rivière-Lorphèvre, E. Filippi, Numerical contribution to the comprehension of saw-toothed Ti6Al4V chip formation in orthogonal cutting, Int. J. Mech. Sci. 81 (2014) 77–87.
[15] G.E. Moore, Cramming more components onto integrated circuits, Electronics 38 (1965).
[16] M. Bäker, The influence of plastic properties on chip formation, Comput. Mater. Sci. 28 (2003) 556–562.
[17] J. Limido, C. Espinosa, M. Salaün, J. Lacome, SPH method applied to high speed cutting modelling, Int. J. Mech. Sci. 49 (2007) 898–908.
[18] L. Olovsson, K. Simonsson, M. Unosson, Selective mass scaling for explicit finite element analyses, Int. J. Numer. Methods Eng. 63 (2005) 1436–1445.
[19] A.M. Prior, Application of implicit and explicit finite element techniques to metal forming, J. Mater. Process. Technol. 45 (1994) 649–656.
[20] G. Cocchetti, M. Pagani, U. Perego, Selective mass scaling and critical time-step estimate for explicit dynamics analyses with solid-shell elements, Comput. Struct. (2012).
[21] P. Wriggers, Nonlinear Finite Element Methods, Springer, 2008.
[22] S. Georgescu, P. Chow, H. Okuda, GPU acceleration for FEM-based structural analysis, Arch. Comput. Methods Eng. 20 (2013) 111–121.
[23] S. Sun, M. Brandt, M. Dargusch, Characteristics of cutting forces and chip formation in machining of titanium alloys, Int. J. Mach. Tools Manuf. 49 (2009) 561–568.
[24] T. Mabrouki, F. Girardin, M. Asad, J.-F. Rigal, Numerical and experimental study of dry cutting for an aeronautic aluminium alloy (A2024-T351), Int. J. Mach. Tools Manuf. 48 (2008) 1187–1197.
[25] O. Pantalé, Plateforme de prototypage virtuel pour la simulation numérique en Grandes Transformations Thermomécaniques Rapides, Technical Report, Institut National Polytechnique de Toulouse, 2005.
[26] M. Calamaz, D. Coupard, F. Girot, A new material model for 2D numerical simulation of serrated chip formation when machining titanium alloy Ti-6Al-4V, Int. J. Mach. Tools Manuf. 48 (2008) 275–288.
[27] G. Johnson, W. Cook, A constitutive model and data for metals subjected to large strains, high strain rates and high temperatures, in: Proceedings of the Seventh International Symposium on Ballistics, The Hague, The Netherlands, 1983, pp. 541–547
[28] T. Özel, E. Zeren, Numerical modelling of meso-scale finish machining with finite edge radius tools, Int. J. Mach. Mach. Mater. 2 (2007) 451–768.
[29] J. Sun, Y.B. Guo, Material flow stress and failure in multiscale machining titanium alloy Ti-6Al-4V, Int. J. Adv. Manuf. Technol. 41 (2009) 651–659.
[30] D.R. Lesuer, Experimental Investigations of Material Models for Ti-6Al-4V Titanium and 2024-T3 Aluminum, Technical Report, Lawrence Livermore National Laboratory, 2000.
[31] F. Ducobu, E. Rivière-Lorphèvre, E. Filippi, A Lagrangian FEM model to produce saw-toothed macro-chip and to study the depth of cut influence on its formation in orthogonal cutting of Ti6Al4V, ARM 223 (2011) 3–11.
[32] S. Lampman, Wrought titanium and titanium alloys, Properties and Selection: Nonferrous Alloys and Special-Purpose Materials, vol. 2, ASM Handbook, 1990.
[33] M. Bäker, J. Rösler, C. Siemers, The influence of thermal conductivity on segmented chip formation, Comput. Mater. Sci. 26 (2003) 175–182.

[34] M. Nasr, E.-G. Ng, M. Elbestawi, Effects of workpiece thermal properties on machining-induced residual stresses – thermal softening and conductivity, Proc. IMechE B: JEM 221 (2007) 1387–1400.
[35] S. Koric, L. Hibbeler, B. Thomas, Explicit coupled thermo-mechanical finite element model of steel solidification, Int. J. Numer. Methods Eng. 78 (2009) 1–31.
[36] K.-J. Bathe, E. Wilson, Numerical Methods in Finite Element Analysis, Prentice-Hall, 1976.
[37] K. Hibbit, Sorenson, Abaqus Analysis User's Manual, Version 6.8, Dassault Systèmes, 2008.
[38] M. Wang, H. Yang, Z. Sun, L. Guo, X. Ou, Dynamic explicit FE modeling of hot rolling process, Trans. Nonferrous Met. Soc. China 16 (2006) 1274–1280.
[39] A. Powell, Finite Difference Solution of the Heat Equation, Technical Report, 2002.
[40] L. Zybell, Finite Element Analysis of Ductile Fracture Behaviour of Pipe Sections with Surface Crack, Technical Report, NTNU, Trondheim, 2005.
[41] L. Wang, H. Long, Investigation of material deformation in multi-pass conventional metal spinning, Mater. Des. 32 (2011) 2891–2899.
[42] J. Wang, C. Huang, W. Song, The effect of tool flank wear on the orthogonal cutting process and its practical implications, J. Mater. Process. Technol. 142 (2003) 338–346.
[43] G. Chryssolouris, Manufacturing Systems: Theory and Practice, Springer, 2006.
[44] C. Doukas, P. Stavropoulos, A. Papacharalampopoulos, P. Foteinopoulos, E. Vasiliadis, G. Chryssolouris, On the estimation of tool-wear for milling operations based on multisensorial data, in: (CIRP CMMO) Procedia CIRP, 14th CIRP Conference on Modelling of Machining Operations, Turin, Italy.
[45] V. Schulze, J. Michna, F. Zanger, R. Pabst, Modeling the process-induced modifications of the microstructure of work piece surface zones in cutting processes, Adv. Mater. Res. 223 (2011) 371–380.
[46] Y.-C. Yen, J. Söhner, B. Lilly, T. Altan, Estimation of tool wear in orthogonal cutting using the finite element analysis, J. Mater. Process. Technol. 146 (2004) 82–91.
[47] L. Xie, J. Schmidt, C. Schmidt, F. Biesinger, 2D FEM estimate of tool wear in turning operation, Wear 258 (2005) 1479–1490.
[48] L. Filice, F. Micari, L. Settineri, D. Umbrello, Wear modelling in mild steel orthogonal cutting when using uncoated carbide tools, Wear 242 (2007) 545–554.
[49] A. Attanasio, E. Ceretti, S. Rizzuti, D. Umbrello, F. Micari, 3D finite element analysis of tool wear in machining, CIRP Ann.-Manuf. Technol. 57 (2008) 61–64.
[50] A. Attanasio, D. Umbrello, Abrasive and diffusive tool wear FEM simulation, Int. J. Mater. Form. 2 (2009) 543–546.